NUMERICAL SOLUTION OF THE LINEARIZED EULER EQUATIONS USING HIGH ORDER FINITE DIFFERENCE OPERATORS WITH THE SUMMATION BY PARTS PROPERTY

Stefan Johansson

Department of Information Technology
Scientific Computing
Uppsala University
P.O. Box 337
SE 75105, Uppsala
Sweden

Abstract

We have used high order finite difference methods with the summation by parts property (SBP) on the 1D linearized Euler equations. The boundary conditions are imposed with both the projection method and the simultaneous approximation term method (SAT) for comparison. The formal fourth order of accuracy of the high order SBP operator was verified with both the projection method and the SAT method. Some relatively large errors were observed at the artificial boundaries and further investigations are needed to improve the non-reflecting boundary conditions.

Key words: linearized Euler equations, computational aeroacoustics, high order difference method, summation by parts, non-reflecting boundary conditions

1 Introduction

Most natural phenomena of interest are governed by partial differential equations (PDEs), yet no general technique is known to find the exact solution to a given well-posed PDE. Therefore numerical methods have been used even long before the birth of digital computers, see for example the work by L. F. Richardson [9].

PDEs governing acoustics often require high order methods to reach accuracy requirements: low dissipation and dispersion errors, cf. Tam [11].

To exemplify there are large scale disparities between the eddy scale l and the acoustic wavelength $\lambda \sim lM^{-1}$, where M is the Mach number. There are also large energy density disparities between the hydrodynamic near field and the acoustic far field cf. [4].

A technique that can be used to avoid resolving the different scales was proposed by Lighthill [7] in the 1950's where one first solves the flow field and uses that solution as a source term to the wave equation to get the acoustic field.

The linearized Euler equations have received interest since they can be used to model refractional effects and reflections at solid boundaries cf. M. Billson et al. [1]. Direct simulation of these phenonema has come into reach for our computers only in recent years.

In the numerical experiments I have studied isentropic and non isentropic sound propagation, governed by the linearized Euler equations in one space dimension. Discretization was done with a finite difference method, more precisely with a high order summation by parts operator (SBP) [6][10]. The boundary conditions were imposed with the simultaneous approximation term method (SAT) introduced by Carpenter et al. [2] and in some cases by the projection method described by Olsson [8]. The classical four step Runge-Kutta method was used for time marching.

The most important advantage of the summation by parts operators is that they lead to strictly stable high order finite difference methods.

The goal of this investigation was to check the accuracy of the summation by parts operator for the linearized Euler equations and to compare the simultaneous approximation term method and the projection method both used to impose boundary conditions.

2 The governing equations

The 1D nonlinear Euler equations read

$$\mathbf{u}_t + \mathbf{A}\mathbf{u}_x = 0 \tag{1}$$

where $\mathbf{u} = (\rho, u, p)^T$ and

$$\mathbf{A} = \begin{pmatrix} u & \rho & 0 \\ 0 & u & 1/\rho \\ 0 & \gamma p & u \end{pmatrix} \tag{2}$$

where u is the velocity, p is the pressure and ρ is the density. Time is denoted by t, x is the space coordinate and γ is the ratio of specific heats, here $\gamma = 1.4$ for air. We then linearize around the mean values (R, U, P). We replace u by $U + \epsilon u'$ and analogous for p and ρ, and neglect high order terms of $\mathcal{O}(\epsilon^2)$ and get

$$\mathbf{u}'_t + \mathbf{B}\mathbf{u}'_x = 0 \tag{3}$$

where $\mathbf{u}' = (\rho', u', p')^T$ and

$$\mathbf{B} = \begin{pmatrix} U & R & 0 \\ 0 & U & 1/R \\ 0 & \gamma P & U \end{pmatrix} \tag{4}$$

The eigenvalues of $\mathbf{B}$ are $U - a$, U and $U + a$, the corresponding eigenvectors are the columns in the matrix

$$\mathbf{R} = \begin{pmatrix} R/a & 1 & R/a \\ -1 & 0 & 1 \\ Ra & 0 & Ra \end{pmatrix} \tag{5}$$

with inverse

$$\mathbf{R^{-1}} = \begin{pmatrix} 0 & -1/2 & 1/(2Ra) \\ 1 & 0 & -1/a^2 \\ 0 & 1/2 & 1/(2Ra) \end{pmatrix} \tag{6}$$

where $a = \gamma P/R$ is the speed of sound. The linearized Euler equations are often used to model sound propagation.

To simplify things we can assume that the change in entropy is zero, the so called isentropic case. Then

$$\frac{p}{p_\infty} = \left(\frac{\rho}{\rho_\infty}\right)^\gamma = \left(\frac{T}{T_\infty}\right)^{\frac{\gamma}{\gamma-1}} \tag{7}$$

where the subscript ∞ denotes a reference state and T is temperature.

The 1D linearized Euler equations for the isentropic case read

$$\mathbf{u}'_t + \mathbf{C}\mathbf{u}'_x = 0 \tag{8}$$

where

$$\mathbf{C} = \begin{pmatrix} U & a \\ a & U \end{pmatrix} \tag{9}$$

and $\mathbf{u}' = (u', \rho')^T$. U, a, u' and ρ' are the mean flow velocity, mean speed of sound, velocity and density perturbations, respectively. In the following, the prime $'$ to indicate perturbation variables will be omitted i.e. from here on, we use the notation $u = u'$ and $\rho = \rho'$, if not stated otherwise. The eigenvalues of $\mathbf{A}$ are $U - a$ and $U + a$, and the corresponding eigenvectors are the columns in

$$\mathbf{R} = \frac{1}{\sqrt{2}} \begin{pmatrix} 1 & 1 \\ 1 & -1 \end{pmatrix}. \tag{10}$$

Define $\mathbf{w} = \mathbf{R}^{-1}\mathbf{u}'$ then we can multiply the above systems (3) and (8) from the left by $\mathbf{R^{-1}}$ to get

$$\mathbf{w}_t + \mathbf{\Lambda} \mathbf{w}_x = 0 \tag{11}$$

where $\mathbf{\Lambda}$ is a diagonal matrix containing the eigenvalues λ_i of $\mathbf{B}$ and $\mathbf{C}$, respectively.

The reason for transforming the system is to be able to use the SAT method described in section 5 for implementing non-reflecting boundary conditions and derive exact solutions.

3 Summation by parts operators

When doing numerical calculations we must establish an upper bound on the growth of the solution. In the continuous case the energy method is often used, for example, with the usual L^2 scalar product and norm

$$(u, v) = \int_a^b uv \, dx \,, \quad ||u|| = (u, u)^{1/2}. \tag{12}$$

We have for the simplest hyperbolic equation, sometimes called the Kreiss equation,

$$u_t = u_x \tag{13}$$

the following energy growth

$$\frac{1}{2}\frac{d||u||^2}{dt} = (u, u_t) = (u, u_x) = \frac{1}{2}[u^2]_a^b. \tag{14}$$

That is the energy growth in time is governed by the boundary values. In the last step, we used integration by parts

$$(u, v_x) = [uv]_a^b - (u_x, v) \tag{15}$$

In the discrete case we want to find an operator $\mathbf{D}$ and a scalar product H that approximates the derivative d/dx and the integral $\int_a^b$ with the same properties as the continuous case.

$$(u, \mathbf{D}v)_h = u_n v_n - u_0 v_0 - (\mathbf{D}u, v)_h \tag{16}$$

where

$$(u, v)_h = h u^T \mathbf{H} v, \text{ where } h \text{ is the step size.} \tag{17}$$

Since equation (16) is the discrete analogue of equation (15), it is called summation by parts property.

An example of such an operator D and scalar product H is

$$\mathbf{D} = \frac{1}{h}\begin{pmatrix} -1 & 1 & 0 & \dots & 0 \\ -0.5 & 0 & 0.5 & \ddots & \vdots \\ 0 & \ddots & \ddots & \ddots & 0 \\ \vdots & \ddots & -0.5 & 0 & 0.5 \\ 0 & \dots & 0 & -1 & 1 \end{pmatrix}, \mathbf{H} = \begin{pmatrix} 0.5 & 0 & \dots & & 0 \\ 0 & 1 & 0 & & \\ \vdots & \ddots & \ddots & \ddots & \vdots \\ & & 0 & 1 & 0 \\ 0 & & \dots & 0 & 0.5 \end{pmatrix}.$$

Operators if this kind were described by Kreiss and Scherer [6], and high order operators were later constructed by Strand [10]. High order operators $\mathbf{D}$ have the following structure: in the interior a standard centered high order finite difference stencil is used and near the boundary when the standard stencil cannot be used, a small dense matrix is used instead. E.g. the boundary matrix giving third order is 6×9. The stencil giving sixth order and that boundary matrix giving third order are given in the Appendix. For diagonal norms $\mathbf{H}$ Strand [10] constructed matrices $\mathbf{Q}$ giving order $s = 1, \dots, 4$ corresponding to stencils of order $2s$ in the interior.

4 Projection method

To apply high order operators of the SBP type to an initial boundary value problem (IVBP) the analytical boundary conditions must be satisfied in a certain way in order not to destroy the SBP property. Currently there are two popular methods, the projection method and the simultaneous approximation term (SAT) method. The latter method will be described in the next section. The theory of the projection method can be found in [8] and is outlined here. Olsson's idea was that the boundary condition was fulfilled by projecting the discrete solution to the initial value problem to the vector space where it is fulfilled. Using SBP operators he could give an energy estimate for the semi-discrete case.

Let the boundary condition be written in the form

$$\mathbf{L}^T v = g \tag{18}$$

were $\mathbf{L}$ is a rectangular matrix, v the vector of unknowns and $g = g(t)$ a known function. Then the matrix

$$\mathbf{P} = \mathbf{I} - \mathbf{H}^{-1}\mathbf{L}(\mathbf{L}^T\mathbf{H}^{-1}\mathbf{L})^{-1}\mathbf{L}^T \tag{19}$$

where I is the identity matrix, defines a projection with the following properties

- $\mathbf{P}^2 = \mathbf{P}$
- $\mathbf{HP} = \mathbf{P}^T\mathbf{H}$
- $v = \mathbf{P}v \Leftrightarrow \mathbf{L}^T v = 0$.

Given the linear advection equation

$$u_t + cu_x = 0 \tag{20}$$

were c is the advection speed. The projection method for the semi discrete problem becomes

$$v_t + \mathbf{P}c\mathbf{D}v = 0 \quad (21)$$
$$v(0) = f \quad (22)$$

where f is the initial condition. In general the right hand side in (21) involves time derivatives of g, but in our case it is zero because we implement non-reflecting boundary conditions.

Given two matrices $\mathbf{A}_{m,n}$ and $\mathbf{B}_{p,q}$. The Kronecker product $\otimes$ is defined as

$$\mathbf{A} \otimes \mathbf{B} = \begin{pmatrix} a_{1,1}\mathbf{B} & \dots & a_{1,n}\mathbf{B} \\ \vdots & & \vdots \\ a_{m,1}\mathbf{B} & \dots & a_{m,n}\mathbf{B} \end{pmatrix}.$$

For systems the projection method can be expressed using the Kronecker product

$$v_t + (\mathbf{I} \otimes \mathbf{P})(\mathbf{I}_{N,N} \otimes \mathbf{C})(\mathbf{D} \otimes \mathbf{I})v = 0 \quad (23)$$
$$v(0) = f \quad (24)$$

were $\mathbf{I}_{N,N}$ is the identity matrix of dimension $N \times N$, $\mathbf{C}$ is the diagonal matrix $diag[c, \dots, c]^T$ the dimension of the identity matrix $\mathbf{I}$ is the same as the number of equations (in our case we have two equations) in the system, and the values in v and f are ordered vector wise, for example $v = [u_0, \rho_0, u_1, \rho_1, \dots, u_N, \rho_N]^T$.

5 Simultaneous approximation term

In the SAT method one does not impose the exact boundary conditions (b.c.) which might destroy the SBP property and can lead to time-instabilities i.e. the solution can suddenly blow up if you calculate long enough in time. Instead the boundary conditions are imposed as a penalty term at the same accuracy as the discretization. Below is the SAT formulation for (3) and is analogous for (8). We start with the semi-discrete form of (3).

$$\mathbf{v}_t + \mathbf{D} \otimes \mathbf{B}\mathbf{v} = 0 \quad (25)$$

and for systems the SAT method reads:

$$\mathbf{v}_t + (I_{N,N} \otimes \mathbf{B})(\mathbf{D} \otimes I)\mathbf{v} = SAT \quad (26)$$

were $I_{N,N}$ is the identity matrix of dimension $N \times N$, n is the number of equations in the system, the dimension of the identity matrix I is n, and the values in v are ordered vector wise, for example $\mathbf{v} = [u_0, \rho_0, u_1, \rho_1, \dots, u_N, \rho_N]^T$. where

$$SAT_j = \begin{cases} -h_{00}^{-1}\mathbf{R}(\mathbf{\Lambda}^+\mathbf{R}^{-1}v_0 - \Phi_0(t))h^{-1}, & \text{j=0,} \\ 0, & 0 < j < N, \\ h_{NN}^{-1}\mathbf{R}(\mathbf{\Lambda}^-\mathbf{R}^{-1}v_N - \Phi_N(t))h^{-1}, & \text{j=N,} \end{cases} \quad (27)$$

h_{00} and h_{NN} are the first and last elements of the norm matrix H and $\mathbf{\Lambda}^{\pm} = \frac{1}{2}(\Lambda \pm |\Lambda|)$, with $|\Lambda| = diag(|\lambda_i|)$. Non-reflecting boundary conditions are implemented by $\Phi_0(t) = \Phi_N(t) = 0$

6 The classical Runge-Kutta method for ODE's

Using a summation by parts operator in the system

$$u_t + \mathbf{A}u_x = 0 \tag{28}$$

gives a large system of ODE's

$$v_t = \mathbf{P}v \tag{29}$$

were $\mathbf{P}$ is a discrete approximation of $-\mathbf{A}\frac{d}{dx}$.

To solve this system we use the classical Runge-Kutta method [3], which is fourth order accurate.

$$v^{(1)} = v^n \tag{30}$$

$$v^{(2)} = v^n + \frac{1}{2}\Delta t\mathbf{P}v^{(1)} \tag{31}$$

$$v^{(3)} = v^n + \frac{1}{2}\Delta t\mathbf{P}v^{(2)} \tag{32}$$

$$v^{(4)} = v^n + \Delta t\mathbf{P}v^{(3)} \tag{33}$$

$$v^{n+1} = v^n + \Delta t\left(\frac{1}{6}\mathbf{P}v^{(1)} + \frac{1}{3}\mathbf{P}v^{(2)} + \frac{1}{3}\mathbf{P}v^{(3)} + \frac{1}{6}\mathbf{P}v^{(4)}\right). \tag{34}$$

7 Numerical experiments

The test cases are now described in more detail. The equations used are the linearized isentropic Euler equations(8) and the linearized Euler equations (3), with a sine pulse in the isentropic case and a Gaussian in the non-isentropic case.

7.1 Isentropic test case

The initial values given are

$$u'(x,0) = \begin{cases} (sin\frac{x-0.4}{0.2}\pi)^4 & \text{if } 0.4 \leq x \leq 0.6 \\ 0 & \text{otherwise} \end{cases}$$

The initial density perturbation ρ' is set to zero, and the Mach number $M = U/a$ is 0.5.

The solution to the acoustic velocity field and the acoustic density field there are two waves traveling in opposite directions and at different speeds ($U + a = 1$ and $U - a = -1/3$) see figures 1 and 2. There are no apparent differences in the two methods used to impose the boundary conditions. The convergence rate is close to four when a wave has reached the boundary, as it should be since the overall accuracy is at most one order higher than at the boundary [5]. The same tests were done with the SBP operator of second order with similar results.

Different time steps were also used with the high order SBP operator, varying from $CFL = 0.1$ and $CFL = 0.99$. If a larger CFL number was used the convergence rate dropped somewhat but not below four when the waves were inside the domain and then dropped to about four at the boundary.

Since we have a sixth order stencil in the interior we should expect sixth order accuracy until a wave reaches the boundary, and one explanation may be that the initial condition has a discontinuous derivative.

Some wiggles were observed in the solution see section 7.3, these can be damped using artificial dissipation. This is often necessary when using finite difference methods with no inherent dissipation as with the present SBP operators.

The time instants were chosen such that for the first time both waves were inside the computational domain, for the second time $t = 0.75$ one had reached the boundary and in the last case the first wave had left the domain and the second had reached the other boundary. In some test runs the computation continued until $T = 20$ to check for long time stability. Some small wiggles were observed in the solution due to the fact that no artificial dissipation was added to the numerical scheme, and also due to the fact that the initial condition has a discontinuous first derivative. In more realistic test cases artificial dissipation has to be added to damp high frequency oscillations.

Results using the projection method can be seen in table 1. The convergence rate is computed with respect to a grid with half as many points. The columns give the results from three time instants 0.25, 0.75 and 1.5.

Table 1: Order of accuracy for SBP 3-6 using the projection method for the isentropic Euler equations

# of grid points / Time	0.25	0.75	1.5
100			
200	4.7253	4.0004	3.9834
400	4.4069	4.0140	4.0369
800	4.2376	4.0138	4.0453

Results using the simultaneous approximation term method can be seen in table 2. The convergence rate is computed with respect to a grid with half as many points. The columns give the results from three time instants 0.25, 0.75 and 1.5.

Table 2: Order of accuracy for SBP 3-6 using the simultaneous approximation term method for the isentropic Euler equations

# of grid points / Time	0.25	0.75	1.5
100			
200	4.7253	4.0004	3.9885
400	4.4069	4.0140	4.0779
800	4.2376	4.0138	4.0961

For both the projection and SAT method we observe an overall forth order accuracy, as should be expected. More surprising is that the order of accuracy is not close to six when no wave has reached the boundary. Later experiments indicated that reason for the lower accuracy was caused by the non-smooth initial condition, cf. section 7.3.

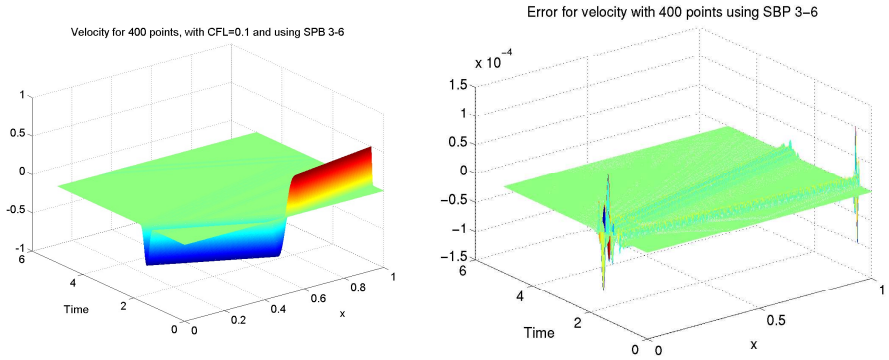

Figure 1: Acoustic velocity and error fields for the isentropic linearized 1D Euler equations using 400 points in the x-direction.

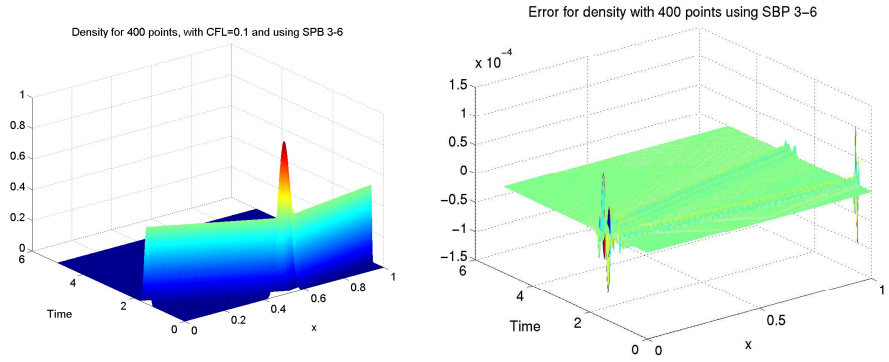

Figure 2: Density perturbations and error fields for the isentropic linearized 1D Euler equations using 400 points in the x-direction.

The large errors observed at the boundaries in figures 1 and 2 were unexpected, because one had expected an error at the boundary that was comparable to the error inside the computational domain. Future investigation will deal with this problem.

7.2 Non-isentropic test case

7.2.1 Left going acoustic wave

The initial values are now instead given by

$$u'(x,0) = \alpha e^{(-\beta(x-0.5)^2)} \quad (35)$$

$$p'(x,0) = -Rau'(x,0) \quad (36)$$

$$\rho'(x,0) = -Ru'(x,0)/a \quad (37)$$

where the parameters are chosen as $\alpha = 1$ and $\beta = 250$. The Mach number is chosen to be 0.5.

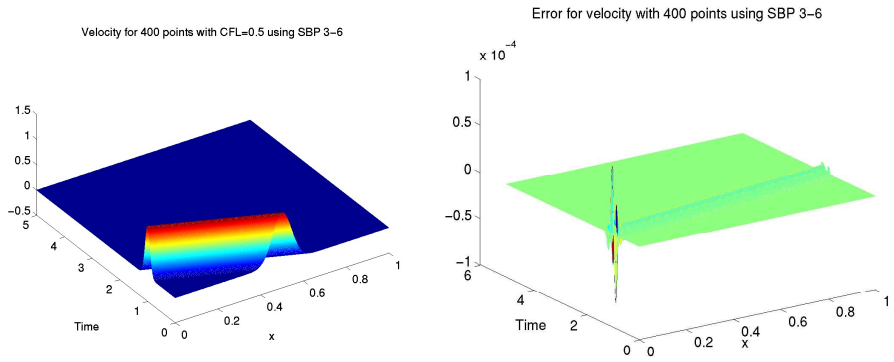

Figure 3: Acoustic velocity end error fields for the non isentropic linearized 1D Euler equation using 400 points in the x-direction, respectively.

The wave in figure 3 is moving to the left and therefore corresponds to the eigenvalue $U - a$. The only Riemann invariant that is non zero with the initial values used is the one corresponding to the same eigenvalue. The characteristic variables are given by multiplying the primitive variables i.e. $\rho, u,$ and p with the inverse of the eigenvector matrix from the left.

Table 3: Order of accuracy for SBP 3-6 using the simultaneous approximation term method for the non-isentropic Euler equations, with left going acoustic wave.

# of grid points /Time	0.25	0.75	1.5
100			
200	5.8772	5.7965	3.9386
400	5.8238	5.7486	3.9602
800	5.6634	5.5458	3.9678

In table 3 the time instants 0.25, 0.75 and 1.5 were the same as for the isentropic case for convenience. For the first two time instants the wave is still inside the domain, and has left at the third. Now we observe about sixth order of accuracy, when no information has reached the boundary as we should expect.

7.2.2 Right going acoustic wave

The initial values are now given by

$$u'(x,0) = \alpha e^{(-\beta(x-0.5)^2)} \quad (38)$$
$$p'(x,0) = Rau'(0,x) \quad (39)$$
$$\rho'(x,0) = Ru'(x,0)/a \quad (40)$$

where the parameters are chosen as, $\alpha = 1$ and $\beta = 250$. The Mach number is chosen to be 0.5.

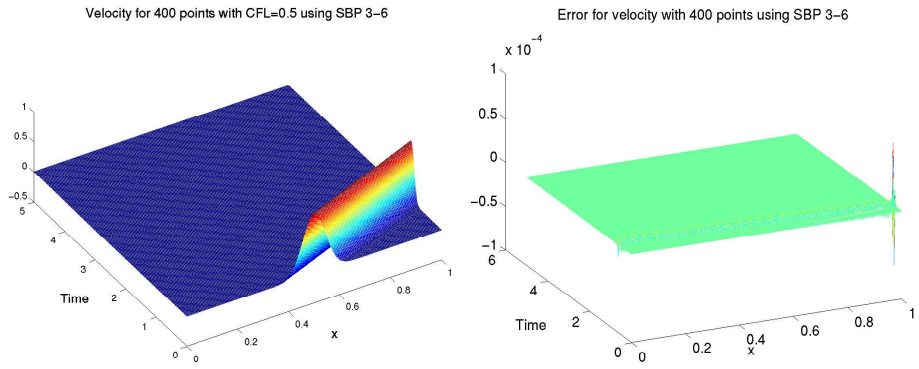

Figure 4: Acoustic velocity and error fields for the non isentropic linearized 1D Euler equation using 400 points in the x-direction, respectively.

The wave in figure 4 is moving to the right and therefore corresponds to the eigenvalue $U + a$. The only Riemann invariant that is non zero with the initial values used is the one corresponding to the same eigenvalue.

Table 4: Order of accuracy for SBP 3-6 using the simultaneous approximation term method for the non-isentropic Euler equations, with right going acoustic wave.

# of grid points /Time	0.05	0.15	0.3
100			
200	5.9284	5.9189	3.9354
400	5.9424	5.9353	3.9585
800	5.8441	5.8203	3.9667

The reason for using different time instants was the greater speed of the right going wave. So in order to capture it inside the domain smaller time instants had to be used. At the first two time instants 0.05 and 0.15 the wave is still inside the domain and at the last instant 0.3 it has left the computational domain.

As before we compare the numerical solution with the exact solution and the results are similar to the isentropic case. Except of course the observed close to sixth order accuracy when the wave was still inside the domain cf. table 4.

7.2.3 Right going entropy wave

The initial values are now given by

$$u'(x,0) = 0 \quad (41)$$
$$p'(x,0) = 0 \quad (42)$$
$$\rho'(x,0) = \alpha e^{(-\beta(x-0.5)^2)} \quad (43)$$
$$(44)$$

where the parameters are chosen as $\alpha = 1$ and $\beta = 250$. The Mach number is chosen to be 0.5. For the above initial conditions only the density ρ' is non zero.

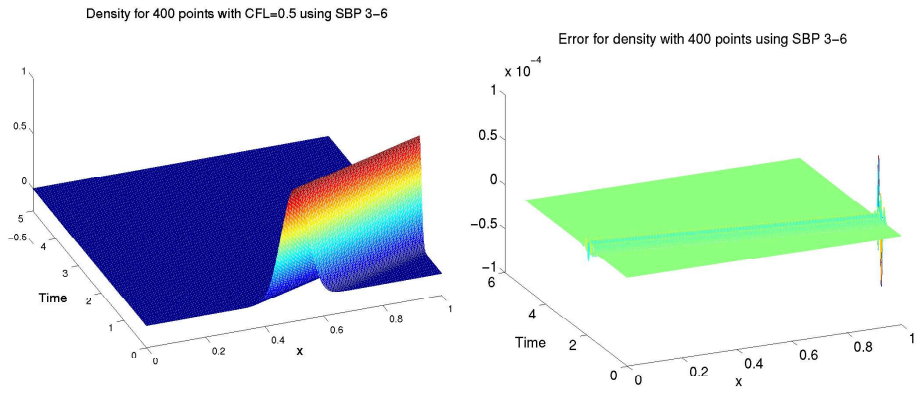

Figure 5: Acoustic density and error fields for the non isentropic linearized 1D Euler equation using 400 points in the x-direction, respectively.

Table 5: Order of accuracy for SBP 3-6 using the simultaneous approximation term method for the non-isentropic Euler equations, with right going entropy wave.

# of grid points /Time hline 100	0.25	0.75	1.5
200	5.9243	5.9148	4.0473
400	5.9324	5.9253	4.0852
800	5.8960	5.8899	4.0885

In the above experiment see figure 5 and table 5, we have chosen the initial condition such that only one Riemann invariant, namely entropy, was non-zero.

All three test cases for the non-isentropic Euler equations displayed sixth order accuracy and fourth order when the wave reaches the boundary as theory predicts. Also the wiggles that were observed in the isentropic case with the non-smooth initial condition were not observed and are discussed in the following section.

7.3 Comparison between $\mathcal{C}^0$ and $\mathcal{C}^\infty$ initial data

For the isentropic case the following $\mathcal{C}^0$ initial data was used cf. figure 6

$$u'(x,0) = \begin{cases} (sin\frac{x-0.4}{0.2}\pi)^4 & \text{if } 0.4 \leq x \leq 0.6 \\ 0 & \text{otherwise.} \end{cases}$$

and the initial density perturbation ρ' is set to zero. As before the Mach number $M = U/a$ was chosen to be 0.5.

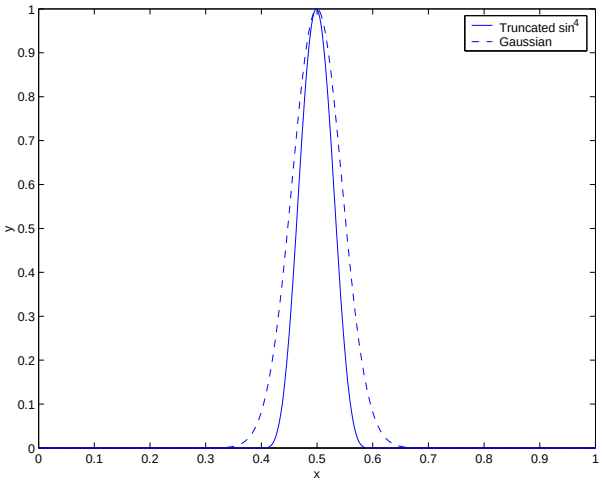

Figure 6: The two initial conditions, solid for the truncated sin^4 curve and dashed for the Gaussian curve.

Due to the discontinuity in the first derivative there are wiggles in the solution as can be seen in Fig. 7. The discontinuity leads to high frequency oscillations in the Fourier domain that cannot be represented by the finite difference method.

These wiggles are not present when we use the $\mathcal{C}^\infty$ initial data that were used in the non isentropic case

$$u'(x,0) = \alpha e^{(-\beta(x-0.5)^2)}$$

with $\alpha = 250$ and $\beta = 0.5$.

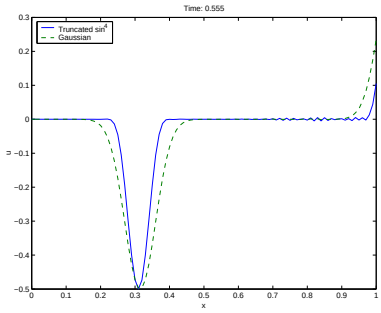

(a) The fastest acoustic wave is leaving the domain, notice the wiggles at the right boundary.

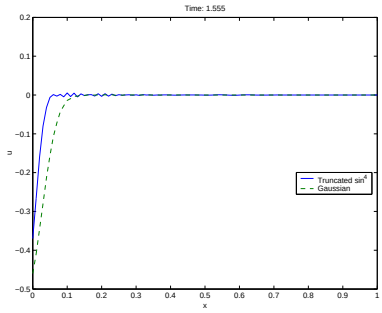

(b) The second, slower acoustic wave is leaving, and again notice the wiggles at the left boundary this time.

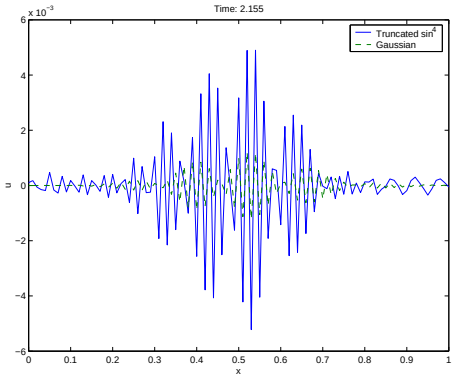

(c) Both waves have left the domain, presented for completeness.

Figure 7: Numerical solution using different initial data, solid denotes the one with truncated sin^4 and dashed the Gaussian curve.

We have seen the high frequency oscillations that occur in the numerical solution when using the truncated sin^4 curve as initial condition. These oscillations are most likely the cause of the fact that sixth order accuracy was not observed when no wave had reached the boundary in the isentropic case.

7.4 Comparison between SBP 1-2 and SBP 3-6

The summation by parts operator SBP 3-6 has third order accuracy at the boundary and therefore the overall accuracy is fourth order[5]. The SBP 1-2 operator therefore is of second order accuracy, the figures 8 and 9 show the error compared to the exact solution.

The time to solve the non isentropic Euler equations using with SBP 3-6 is only about 50 % more per time step than with SBP 1-2, and the figure 8 shows the advantage of the high order method on this case.

For the SBP 3-6, the error is about one order of magnitude smaller until the wave reaches the boundary were the error has a jump. When the wave leaves the boundary the accuracy is not sixth order as it was in the interior but fourth order.

When using the SBP 1-2 it is also apparent that the error grows linearly with time, this can also be seen when zooming in on 9. This can be observed with all finite difference methods.

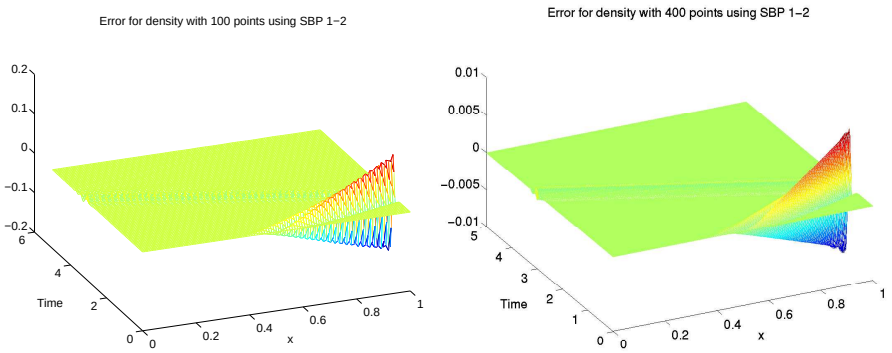

Figure 8: The error with time for the density with 100 and 400 points using SBP 1-2.

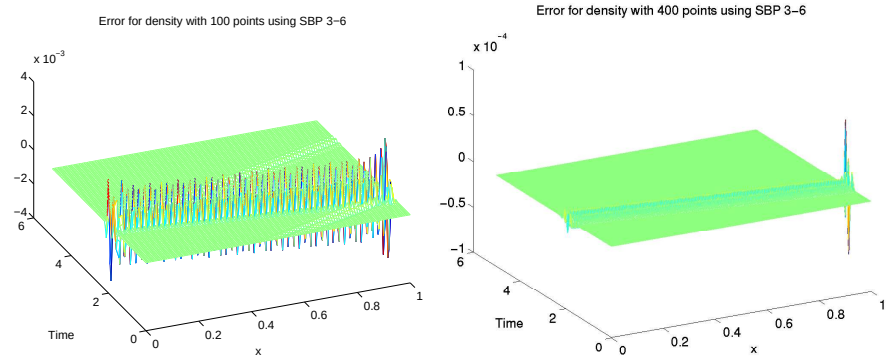

Figure 9: The error with time for the density with 100 and 400 points using SBP 3-6.

7.4.1 Mach number dependence

In order to investigate the Mach number dependence on the numerical solution a test case was chosen with Mach number equal to 0.1. The initial values are

now given by

$$u'(x,0) = \alpha e^{(-\beta(x-0.5)^2)} \quad (45)$$

$$p'(x,0) = -\alpha e^{(-\beta(x-0.5)^2)} \quad (46)$$

$$\rho'(x,0) = \alpha e^{(-\beta(x-0.5)^2)} \quad (47)$$

where the parameters are chosen as $\alpha = 1$ and $\beta = 250$.

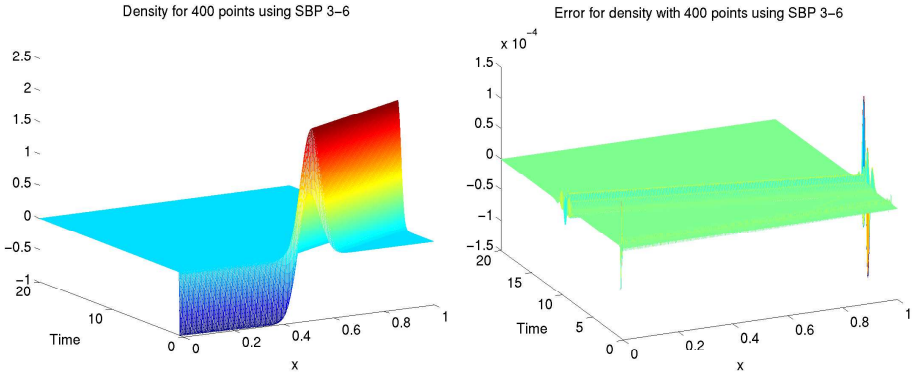

In the previous test cases for the non-isentropic Euler equations there are now three waves present a left and a right going acoustic wave and a right going entropy wave.

The same behavour is observed as for the three test cases for the linear non-isentropic Euler equations with Mach number 0.5. That is that there are some problems at the boundaries which were not anticipated. Other then that the only difference is that the calculations must be run for longer time in order to let the slowest wave leave the domain, namely the entropy wave.

8 Conclusions

The summation by parts operators of overall fourth order are used together with the projection method and the simultaneous approximation term method to implement the boundary conditions and the classical fourth order Runge-Kutta method for time-stepping. The isentropic linearized 1D Euler equations and the non isentropic linearized 1D Euler equations are considered. Note that the projection method was not used for the non isentropic linearized Euler equations.

No noticeable differences were observed between the projection or simultaneous approximation term method, neither in accuracy or time to solve the problem for the isentropic linearized Euler equations.

A comparison between summation by parts operators with different orders of accuracy showed that a 50 % increase in computation time for the high order method reduced the error by about two orders magnitude compared with the second-order method.

The errors of the reflected numerical waves are considerably larger then the errors of the outgoing physical waves. These problems at the boundary

that were observed with the high order method were not anticipated. However, when the same method and boundary conditions were implemented for the scalar Kreiss equation, the same problem at the boundary was found. One possible explanation of the problem is that the discrete method allows for unphysical waves traveling in the wrong direction, which the boundary conditions will not handle properly. Further investigations will be conducted to determine the source of the problem.

9 Appendix

The SBP operator with sixth order accuracy in the interior and third near the boundary (SBP 3-6) has a standard centered finite difference operator in the interior of **D**

$$D(j,j-3) = -\frac{1}{60h}, \quad D(j,j-2) = \frac{3}{20h}, \quad D(j,j-1) = -\frac{3}{4h},$$
$$D(j,j) = 0, \quad D(j,j+1) = \frac{3}{4h}, \quad D(j,j+2) = -\frac{3}{20h},$$
$$D(j,j+3) = \frac{1}{60h} \quad \text{for } j = 7,\ldots,N-6$$

H is a diagonal matrix with ones in the diagonal except for some elements in the beginning and end of the diagonal. In this case the first ones read 13649/43200 12013/8640 2711/4320 5359/4320 7877/8640 and 43801/43200, and in reverse order at the end.

Below is the boundary operator for **D** in the SBP 3-6 operator, namely `D(1:6,1:9) = Q/h`. The indices refer to indices in **D** but the same operator is located in the bottom right half corner with opposite sign and the elements are in a different order as the MATLAB code shows.

```
D(N-5:N,N-8:N) = -Q(6:-1:1,9:-1:1)/h;
```

Q(1 , 1)= -1.5825335189391164188
Q(1 , 2)= 1.9968007424231323418
Q(1 , 3)= $.47988863653014872884 * 10^{-2}$
Q(1 , 4)= $-.66986592424353432486$
Q(1 , 5)= $.25079981439421691455$
Q(1 , 6)= 0
Q(1 , 7)= 0
Q(1 , 8)= 0
Q(1 , 9)= 0
Q(2 , 1)= $-.45374732928216654180$
Q(2 , 2)= 0
Q(2 , 3)= $.20413995948833208469$
Q(2 , 4)= $.42505341435666916396$
Q(2 , 5)= $-.19379006076750187297$
Q(2 , 6)= $.18344016204667166126 * 10^{-1}$
Q(2 , 7)= 0
Q(2 , 8)= 0
Q(2 , 9)= 0
Q(3 , 1)= $-.24160826263371449650 * 10^{-2}$

Q(3 , 2)= −.45229312676749047092
Q(3 , 3)= 0
Q(3 , 4)= .23791958686831427518
Q(3 , 5)= .34541374646501905816
Q(3 , 6)= −.12862412393950571745
Q(3 , 7)= 0
Q(3 , 8)= 0
Q(3 , 9)= 0
Q(4 , 1)= .17061018846799776078
Q(4 , 2)= −.47641039995023947254
Q(4 , 3)= −.12035827579772345587
Q(4 , 4)= 0
Q(4 , 5)= .42710082726876904895
Q(4 , 6)= $-.14377682403433476395 * 10^{-1}$
Q(4 , 7)= $.13435342414629595074 * 10^{-1}$
Q(4 , 8)= 0
Q(4 , 9)= 0
Q(5 , 1)= $-.86915492361728238331 * 10^{-1}$
Q(5 , 2)= .29554398882823409928
Q(5 , 3)= −.23775972239854428505
Q(5 , 4)= −.58114341331302103170
Q(5 , 5)= 0
Q(5 , 6)= .75652321103635055647
Q(5 , 7)= −.16452964326520248826
Q(5 , 8)= $.18281071473911387584 * 10^{-1}$
Q(5 , 9)= 0
Q(6 , 1)= 0
Q(6 , 2)= $-.25155437851495019140 * 10^{-1}$
Q(6 , 3)= $.79610054564964270222 * 10^{-1}$
Q(6 , 4)= $.17590922581676217438 * 10^{-1}$
Q(6 , 5)= −.68025083141176381057
Q(6 , 6)= 0
Q(6 , 7)= .73970913906075203762
Q(6 , 8)= −.14794182781215040752
Q(6 , 9)= $.16437980868016711947 * 10^{-1}$

References

[1] M. Billson, L.-E. Eriksson, and L. Davidson. Acoustics Source Terms for the Linear Euler Equations on Conservative Form. AIAA Paper, 2002-2582, 2002.

[2] M.H. Carpenter, D. Gottlieb, and S. Abarbanel. Time-Stable Boundary Conditions for Finite-Difference Schemes Solving Hyperbolic Systems: Methodology and Application to High-Order Compact Schemes. *J. Comp. Phys.*, 111:220–236, (1994).

[3] G. Dahlquist and Å. Björck. *Numerical Methods*. Prentice-Hall, 1974.

[4] Crighton D.G. Computational Aeroacoustics For Low Mach Number Flows. In J.C. Hardin and M.Y. Hussaini, editors, *Computational Aeroacoustics*, ICASE/NASA LaRC Series, 1995.

[5] B. Gustafsson. The Convergence Rate for Difference Approximations to Mixed Initial Boundary Value Problems. *Math. Comp.*, 29(130):396–406, (1975).

[6] H.-O. Kreiss and G. Scherer. Finite Element and Finite Difference Methods for Hyperbolic Partial Differential Equations. In C. De Boor, editor, *Mathematical Aspects of Finite Elements in Partial Differential Equations.*, pages 195–211. Academic Press, Inc., (1974).

[7] J. Lighthill. On sound generated aerodynamically. I. General theory. *Proc. of the Royal Soc. of London A*, 211:564–587, (1952).

[8] P. Olsson. Summation by Parts, Projections, and Stability. I. *Math. Comp.*, 64:1035–1065, (1995).

[9] L.F. Richardson. The Approximate Arithmetical Solution by Finite Differences of Physical Problems involving Differential Equations, with an Application to the Stresses in a Masonry Dam. *Philo. Trans. of the Royal Soc. of London*, 210:307–357, (1910).

[10] B. Strand. Summation by Parts for Finite Difference Approximations for d/dx. *J. Comp. Phys.*, 110:47–67, (1994).

[11] C.K.W Tam. Computational aeroacoustics: Issues and methods. *AIAA J.*, 33:1788–1796, (1995).